J. Fluid Mech. (2005), *vol.* 531, *pp.* 191–219. © 2005 Cambridge University Press
doi:10.1017/S0022112005003927 Printed in the United Kingdom

Experimental observations of upstream overdeepening

By GUIDO ZOLEZZI†, MICHELE GUALA, DONATELLA TERMINI‡ AND GIOVANNI SEMINARA

Dipartimento di Ingegneria Ambientale Università di Genova, via Montallegro 1, 16145 Genova, Italy

(Received 4 January 2003 and in revised form 5 October 2004)

The issue of morphodynamic influence in meandering streams is investigated through a series of laboratory experiments on curved and straight flumes. Both qualitative and quantitative observations confirm the suitability of the recent theoretical developments (Zolezzi & Seminara 2001) that indicate the occurrence of two distinct regimes of morphodynamic influence, depending on the value of the width ratio of the channel β. The threshold value β_R separating the upstream from the downstream influence regimes coincides with the resonant value discovered by Blondeaux & Seminara (1985). Indeed it is observed that upstream influence may occur only in relatively wide channels, while narrower streams are dominated by downstream influence. A series of experiments has been carried out in order to check the above theoretical predictions and show, for the first time, evidence of the occurrence of upstream overdeepening. Two different sets of experiments have been designed where a discontinuity in channel geometry was present such that the channel morphodynamics was influenced in the upstream direction under super-resonant conditions ($\beta > \beta_R$) and in the downstream direction under sub-resonant conditions ($\beta < \beta_R$). Experimental results give qualitative and quantitative support to the theoretical predictions and allow us to clarify the limits of the linear analysis.

1. Introduction

In recent years, the engineering of bank protection and regulation works in natural rivers has been given increasing scientific support owing to a greater understanding of the physical mechanisms governing fluvial processes, particularly those related to sediment transport and changes in channel morphology (e.g. Klaassen 2002).

It is well known that the impact of maintenance works or constructions that modify the river configuration can be felt far from their location. Bottom deformation in natural rivers is due to phenomena acting at different spatial and temporal scales. De Vries (1973) has investigated river aggradation and degradation phenomena, occurring at large spatial scales, on the basis of the one-dimensional approach employing the one-dimensional De St Venant equation, the continuity equation for the solid and fluid phases along with appropriate closure relationships. Such a hyperbolic partial differential system admits of the existence of three families of characteristics. Two of

† Present address: Dipartimento di Ingegneria Civile e Ambientale, Università di Trento, Via Mesiano 77, 38050, Trento, Italy.

‡ Present address: Dipartimento di Ingegneria Idraulica e Applicazioni Ambientali, Università di Palermo, viale delle Scienze, 90128 Palermo, Italy.

https://doi.org/10.1017/S0022112005003927 Published online by Cambridge University Press

the associated celerities are invariably positive, while the third is invariably negative. It is then well established that information, in the form of small-amplitude one-dimensional perturbations of the flow field and bed topography, may propagate upstream even when the flow is supercritical ($Fr > 1$). This phenomenon of upstream influence occurs on the relatively slow time scale associated with bed deformation.

Natural river channels, however, most often display also two-dimensional perturbations of bottom topography. Such large-scale bedforms are known as bars and are characterized by periodic sequences consisting of scour and deposition alternatively shifted towards the left and the right banks. Their development has attracted considerable attention as it emerges from theoretical and experimental work carried out in the last three decades. In the case of single thread rivers, with the commonly observed values of the width to depth ratio β, bars generally appear as single row (alternate) bars, and can either migrate or keep fixed. The bed topography in curved channels is the result of an interaction between such migrating and non-migrating (forced) features, which has been investigated both experimentally (Kinoshita & Miwa 1974) and theoretically (Tubino & Seminara 1990) in the case of small-amplitude periodic meanders. Open issues still remain in the case of large-amplitude meanders (Whiting & Dietrich 1993) and of irregular channels.

The formation of migrating bars is associated with an instability mechanism of the system of turbulent flow–cohesionless bottom occurring in almost straight channels (e.g. Colombini, Seminara & Tubino 1987; Schielen, Doelman & de Swart 1993; Lanzoni 2000*a*, *b*) and are referred to as *free bars*. The length of each bar unit is approximately 6–7 channel widths. The presence of abrupt changes in channel geometry (such as discontinuities in curvature, or localized constructions) may trigger the formation of forced bars (Struiksma *et al.* 1985). They are referred to as *spatial bars* (Seminara & Tubino 1992) and the characteristic length of each unit is of the order of fifteen channel widths, about twice that corresponding to free alternate bars.

The most common example of spatial bars is due to the so called 'overdeepening phenomenon', i.e. the spatial transient whereby the scour associated with the point bar configuration establishes in a bend of constant curvature downstream of a straight reach. This effect was first pointed out by Struiksma *et al.* (1985), who observed that overdeepening occurred immediately downstream of the bend entrance. Such experimental observations are correctly reproduced by the two-dimensional linear theories that have been commonly employed to describe the planimetric evolution of river meanders and are essentially based on the model proposed by Ikeda, Parker & Sawai (1981), later improved by Blondeaux & Seminara (1985), an analysis more recently repeated by Johannesson & Parker (1989). Zolezzi & Seminara (2001, hereinafter referred to as ZS) revisited the depth-averaged formulation of the problem of morphodynamics of arbitrarily curved channels and applied their model to the case of overdeepening. While reproducing the phenomenon observed by Struiksma *et al.* (1985), they also discovered that overdeepening may occur in the straight reach located upstream of the bed entrance. In this case, the presence of a sharp change in channel curvature is felt dominantly in the upstream direction, while the point bar configuration establishes almost immediately downstream of the bend entrance. A sketch of the downstream and upstream overdeepening pattern obtained by ZS is given in figure 1.

This is actually an example of a more general issue, concerning the problem of two-dimensional morphodynamic influence in single-thread meandering rivers. ZS find that the width ratio β is the crucial parameter controlling the phenomenon whereby upstream or downstream influence may dominate the morphodynamics.

https://doi.org/10.1017/S0022112005003927 Published online by Cambridge University Press

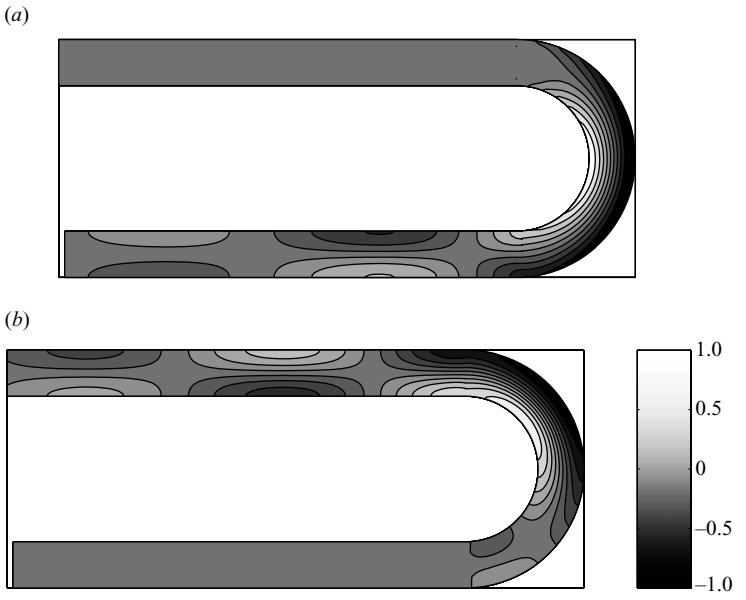


FIGURE 1. The patterns of bed deformation corresponding to (*a*) downstream and (*b*) upstream overdeepening in a 'U-shaped' flume, according to the theory of ZS. The plotted quantity is the local bed elevation scaled by the mean value of the flow depth. Flow from top to bottom of each figure; dark regions denote scour. Calculations based on the parameters of the experiments U2 and D1, respectively (see table 3 and § 5).

More precisely, upstream influence is dominant provided β is larger than a threshold value β_R, that coincides with the resonant value of Blondeaux & Seminara (1985); vice versa, dominant downstream influence occurs when $\beta < \beta_R$. The above mechanism is related to the fact that two-dimensional perturbations, consisting of free migrating bars of small amplitude and suitable large wavelength can migrate upstream under super-resonant conditions provided they are externally forced. Two series of experiments have been carried out in order to test the theoretical prediction of upstream influence. They are the subject of the present paper.

The first series has been carried out on a channel configuration consisting of a straight reach connected with a bend of constant curvature, spanning 270°; we will refer to this as a '270° flume'. A long steady bar has been observed in the upstream reach under super-resonant conditions. However, the upstream reach was not long enough to accommodate one complete bar unit. Nevertheless, these preliminary experiments have allowed us to observe the existence of the phenomenon of upstream influence under super-resonant conditions and its absence under sub-resonant conditions, thus providing a preliminary validation of the conclusions of ZS. These preliminary experiments and their results are described in § 3. A second set of experiments ('U flume' experiments) has then been planned in order to provide a more complete description of channel morphology in the two regimes. The new flume consisted of two longer straight reaches connected by a 180° bend of constant curvature. Observations confirm the occurrence of upstream overdeepening only under super-resonant conditions ($\beta > \beta_R$) showing a good agreement between observed and predicted wavelengths. More generally, the experimental observations point out the existence of two different morphodynamic regimes depending on the value of the width ratio β, as suggested by the theory. Section 4 describes the second series of

https://doi.org/10.1017/S0022112005003927 Published online by Cambridge University Press

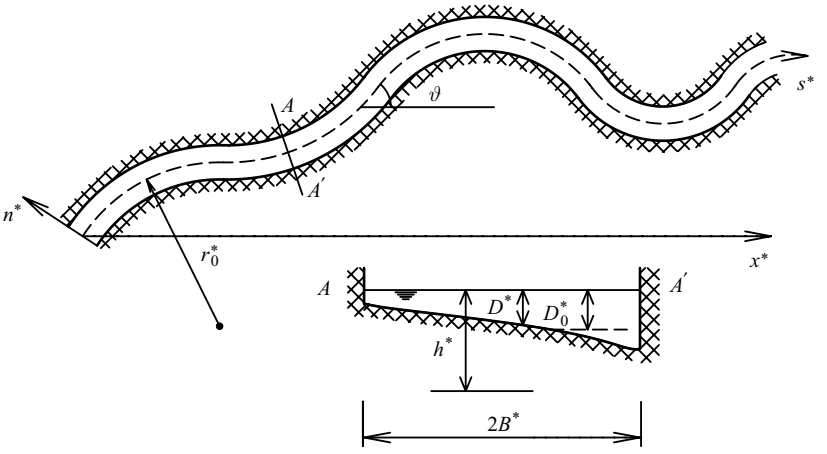


FIGURE 2. Sketch of a meandering channel and notations.

experiments and results are presented in § 5. Finally, § 6 is devoted to some conclusions, along with some discussion of the further developments that will require attention in the future.

2. Theoretical background

A brief outline of the theoretical solution of ZS is given here in order to allow the reader to interpret the present experimental results in terms of the theoretical predictions on the issue of upstream and downstream influence. Let us consider a meandering channel with erodible bottom and constant width, flowing through a floodplain with constant valley slope (figure 2).

The mathematical problem describing the evolution of the flow field and bottom topography is discussed in ZS. Here, we simply recall that the analysis refers to a curvilinear orthogonal coordinate system (s^*, n^*) with s^* the longitudinal coordinate measured along the channel axis and n^* orthogonal to s^* and lying in the valley plane with longitudinal slope S (note that, in the following, a star will denote dimensional quantities). Moreover, $\vartheta(s^*)$ denotes the angle that the local tangent to the channel centreline forms with a given direction, say the downvalley direction, and $\mathscr{C}^*(s^*)$ denotes its curvature. Hence, $\mathscr{C}^*(s^*)$ equals $r^{*-1}(s^*)$, i.e. $-\mathrm{d}\vartheta/\mathrm{d}s^*$, having denoted by $r^*(s^*)$ the local radius of curvature.

The relevant variables of the problem have been made dimensionless as follows: the average half-channel width B^* was employed to scale the planimetric coordinates, while the free-surface elevation H^*, the flow depth D^* and the average sediment size d_s^* were scaled by a reference uniform water depth D_o^*; the depth-averaged velocity vector (U^*, V^*) was scaled by the reference (uniform) flow velocity U_o^* and channel curvature was normalized by the minimum radius of curvature of the river reach R_o^*.

The width ratio β, the curvature ratio ν_o, the Froude number F_o, the Shields stress τ_* and the relative roughness d_s of the reference uniform flow are the relevant dimensionless parameters that read:

$$\beta = \frac{B^*}{D_o^*}, \qquad \nu_o = \frac{B^*}{R_o^*}, \qquad F_o = \frac{U_o^*}{\sqrt{g D_o^*}}, \tag{2.1a–c}$$

$$\tau_* = \frac{S D_o^*}{(s-1) d_s^*}, \qquad d_s = \frac{d_s^*}{D_o^*}. \tag{2.1d, e}$$

https://doi.org/10.1017/S0022112005003927 Published online by Cambridge University Press

River reach	1	2	3	4	5	6	7	8	9	10	11	12
ν_o	0.25	0.19	0.27	0.24	0.19	0.12	0.07	0.11	0.11	0.08	0.12	0.10

TABLE 1. Typical values of the curvature ratio ν_o for natural river reaches, computed from data reported in the following references: 1, Luangwa River, Zambia (Gilvear, Winterbottom & Sichingabula 2000); 2, Oachita River, Arkansas, USA (Biederharn, Raphelt & Montague 1983); 3, 4, reaches 1, 2, of the Sinu River, Colombia (Monsalve & da Silva 1983); 5, Lower Wabash River, Illinois, USA (Ikeda 1989); 6, Buffalo Creek, 7, Cottonwood River, 8, Hawk Creek, 9, Minnesota River, 10, Root River, 11, Wild R River, 12, Yel. Med. River, Minnesota, USA (MacDonald, Parker & Leuthe 1991).

An approximate steady solution of the problem has been derived by ZS in a linear context; the latter assumes that the perturbations of the flow field and bed topography induced by the deviation of the channel axis from the straight configuration stay small relative to the uniform flow configuration. This assumption applies provided the channel curvature is sufficiently small, a feature not uncommon in natural meanders. Table 1 shows that the curvature ratio (a dimensionless measure of the maximum channel curvature) typically attains reasonably small values.

The solution (U, V, D, H) is then expanded in powers of ν_o in the neighbourhood of the reference uniform conditions, truncating the expansion at the first order of approximation, according to a well-established procedure (e.g. Blondeaux & Seminara 1985). Hence,

$$(U, V, D, H) = (U_o, 0, D_o, H_o) + \nu_o(u, v, d, h) + O\left(\nu_o^2\right). \tag{2.2}$$

The perturbations were then decomposed and Fourier analysed as follows:

$$(u, h, d) = \left[0, (\bar{h}\mathscr{C}), (\bar{d}\mathscr{C})\right] n + \sum_{m=0}^{\infty}(u_m, h_m, d_m)\sin(Mn), \quad v = \sum_{m=0}^{\infty} v_m \cos(Mn), \tag{2.3}$$

$$M \equiv \frac{1}{2}(2m+1)\pi. \tag{2.4}$$

Retaining only the first lateral mode in (2.3) and neglecting end effects, the solution found by ZS may be written in the following simplified form:

(*a*) *sub-resonant solution:*

$$\begin{aligned} f = {} & \Gamma_1\mathscr{C}(s) + \Gamma_2\mathscr{C}'(s) + \ldots \\ & + g_1\int_s^L \exp[-\lambda_1(t-s)]\mathscr{C}(t)\,\mathrm{d}t + g_2\int_0^s \exp[-\lambda_2(s-t)]\mathscr{C}(t)\,\mathrm{d}t \\ & + g_3\int_0^s \exp[-\lambda_{3r}(s-t)]\cos[\lambda_{3i}(s-t)-\varphi]\mathscr{C}(t)\,\mathrm{d}t; \end{aligned} \tag{2.5}$$

(*b*) *super-resonant solution:*

$$\begin{aligned} f = {} & \Gamma_1\mathscr{C}(s) + \Gamma_2\mathscr{C}'(s) + \ldots \\ & + g_1\int_s^L \exp[-\lambda_1(t-s)]\mathscr{C}(t)\,\mathrm{d}t + g_2\int_0^s \exp[-\lambda_2(s-t)]\mathscr{C}(t)\,\mathrm{d}t \\ & + g_3\int_0^s \exp[-\lambda_{3r}(t-s)]\cos[\lambda_{3i}(t-s)-\varphi]\mathscr{C}(t)\,\mathrm{d}t, \end{aligned} \tag{2.6}$$

https://doi.org/10.1017/S0022112005003927 Published online by Cambridge University Press

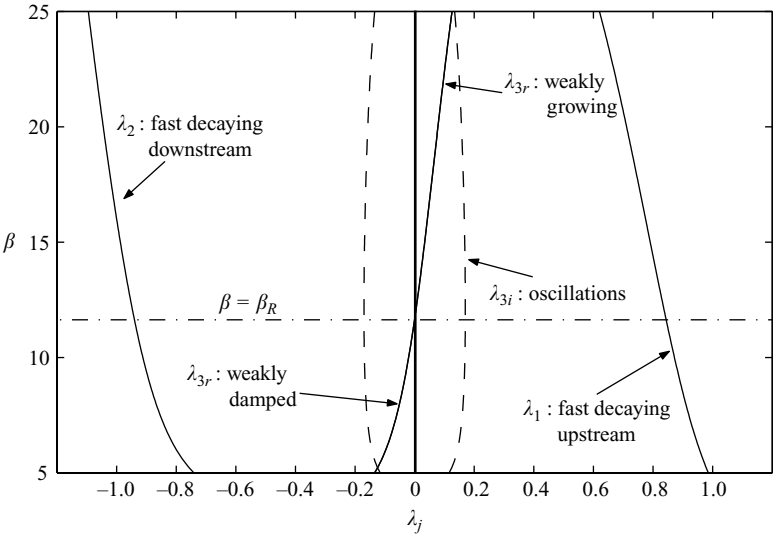


FIGURE 3. The characteristic exponents of the linear solution (2.9) for the first transverse mode ($m = 1$) as functions of the width ratio β for the experimental conditions of run U2 (see table 3).

having denoted by f any of the unknown functions, namely u_1, v_1, h_1 and d_1. In (2.5) and (2.6), Γ_i and g_i ($i = 1, 2, 3$) are functions of the relevant dimensionless parameters (2.1). The important novel features of (2.5) and (2.6) are:

(i) The solution is linearly related not only to the local value of curvature but also to its derivatives (formally up to the eighth, though only the first few terms are significant).

(ii) In the sub-resonant case, the upstream distribution of channel curvature is felt downstream through the second and third convolution integrals of (2.5), with the former decaying fast upstream whereas the latter decays slowly and displays spatial oscillations; the downstream distribution of channel curvature is only weakly felt upstream through the first convolution integral which decays fast upstream.

(iii) In the super-resonant case the situation is reversed: the upstream distribution of channel curvature is weakly felt downstream through the second convolution integral of (2.6) which decays fast downstream, the downstream distribution of channel curvature is felt upstream through the first and third convolution integrals, with the former decaying fast upstream whereas the latter decays slowly and again displays spatial oscillations.

Let us clarify the above statements. The behaviour of the convolution integrals in (2.5) and (2.6) can be understood easily by referring to figure 3 (from ZS) which shows the characteristic exponents λ_j (where $j = 1, \ldots, 3$) for the first dominant transverse mode (alternate bars) as a function of the width ratio β for a given value of the Shields stress τ_* and of the relative roughness d_s. Note that, typically, λ_1 and λ_2 are real numbers while λ_3 is complex. For values of β typical of meandering rivers, the real number λ_1 (λ_2) is always positive (negative), corresponding to upstream (downstream) damped contributions to the solution (2.5) and (2.6). The effect of these contributions, however, is felt within a relatively short reach upstream (downstream) of the given cross section: in fact λ_1 and λ_2 are indeed order-one numbers, hence their influence decays along a distance of the order of a few channel widths.

https://doi.org/10.1017/S0022112005003927 Published online by Cambridge University Press

Contributions associated with the complex exponent (λ_3) oscillate in space with frequency λ_{3i} and decay over a much greater distance, as their damping rate λ_{3r} keeps one order of magnitude lower than λ_1 and λ_2, ranging about 0.1–0.2. These are the most relevant contributions for the determination of the morphodynamic influence: they decay (grow) in the longitudinal direction depending on β falling below (above) a threshold value β_R corresponding to perturbations with vanishing growth rate. The latter coincides with the resonant value originally discovered by Blondeaux & Seminara (1985).

The solution for higher-order modes is similar to (2.5) and (2.6). However, note that, for higher-order modes, the linearity of the solution implies that $\beta_R^{(m)}$ is m times β_R and that:

$$\lambda_j^m(\beta) = m\lambda_j^1\left(\frac{\beta}{m}\right) \qquad (m > 1, \quad j = 1, 2, 3, 4), \tag{2.7}$$

(see Seminara & Tubino 1992). The value of β_R typically ranges around twenty, if the bed is planar or dune-covered (see Seminara & Tubino 1992, figure 4); thus, for higher transverse modes, the values of β_R will be around forty or larger, values typical of braided rivers. As a consequence, the altimetric response of the bed in a meandering (single-channel) river may be characterized by upstream influence only as far as the first mode (corresponding to the alternate bar pattern) is concerned, while the usually smaller higher-order modes are typically characterized by downstream influence. Finally, note that in a linear context, exponentially growing contributions must be discarded as they are unbounded at infinity. This is a severe limitation of the linear approach: in fact, we know from the work of Seminara & Tubino (1992) that spatially growing perturbations may reach a finite equilibrium amplitude: in a nonlinear context growing and decaying perturbations may coexist. Hence, while the linear theory is able to disclose the existence of the phenomenon of upstream influence, the problem of predicting whether the finite-amplitude bars will actually develop will ultimately require a fully nonlinear analysis.

3. Preliminary experiments: occurrence of upstream overdeepening

3.1. 270° *flume apparatus, set-up and data analysis*

Preliminary experiments have been carried out in a 60 cm wide polyvinylchloride (PVC) flume, consisting of a 5 m long straight reach followed by a bend of constant curvature with radius of 2.5 m spanning 270°.

The flume was filled with quartz sand with d_{50}^*, d_{84}^* and d_{16}^* of about 0.5, 0.8 and 0.3 mm, respectively. The flow entered the flume through a 60 cm wide notch in the head tank at the upstream end of the flume. At the downstream end, an adjustable barrier was used to contain the sediment bottom layer and to control the bed elevation at the outlet. The elevation of the free surface at the outlet was also controlled such as to impose uniform flow conditions, i.e. to remove backwater effects. Along both sides of the flume, an approximately 70 cm high rail, with adjustable slope, supported a carriage used for levelling the bed and holding instruments to measure the bed topography and free-surface elevation.

Bed load discharge was supplied through a sediment feed box located at the upstream end of the flume. The steady sediment flux was monitored during the initial phase of any experiment, so as to ascertain the occurrence of equilibrium conditions, identified by the observation of a stable bed slope. In order to minimize the transient,

https://doi.org/10.1017/S0022112005003927 Published online by Cambridge University Press

Run	1	2	5	6	7
β	6	10	20	18.8	17.6
β_R	23	24	14	14.1	14.2
d_s	0.01	0.016	0.033	0.030	0.029
τ_*	0.20	0.17	0.21	0.22	0.24
$S \times 10^{-2}$	0.46	0.46	1.15	1.0	0.96
F_o	0.58	0.56	1.44	1.37	1.4
D_m^* (cm)	5.0	3.0	1.5	1.6	1.7
Q_l^* ($\mathrm{l\,s^{-1}}$)	12.0	6.1	4.6	5.2	5.8

TABLE 2. Relevant parameters of the 270° experiments.

the bed was prepared by means of a scraper attached to the carriage that ran along the rails: the bed was flattened and the predicted equilibrium slope was imposed. The equilibrium slope under uniform flow conditions is immediately determined once the flow discharge, the sediment discharge, the geometry of the channel and the sediment size are and given. We have employed Meyer-Peter and Müller's predictor (in the form given by Chien 1956) for bedload transport and the logarithmic law for the friction coefficient, with absolute roughness equal to $2.5d_s$ after Engelund & Hansen (1967). The initial bottom profile was traced on both sides of the channel in order to check the establishment of such equilibrium conditions, usually occurring after about 2–3 h. The dynamics of bottom evolution was then monitored at intervals of 10–15 min by tracing an average of 20 longitudinal profiles over transparencies glued on each side of the flume. This procedure led to the description of the bed dynamics at the sidewalls over a minimum of two time periods of migrating bars. The coexistence of forced bars, free migrating bars and the overdeepening phenomenon required a spatial and temporal description of bed evolution so as to allow for a detailed analysis of the bottom pattern. Overdeepening, which is associated with the steady component of flow and bottom perturbations, could only be observed by filtering the effect of migrating large-scale bedforms. Data analysis was then performed by employing a zero-up crossing technique to evaluate the time period of migrating bars over which a time-averaging process was operated, for any given spatial location. At the end of each experiment, the bed topography was measured by a laser scanning device mounted on the carriage. The tolerance of the scanner was 0.1 mm; the spatial mesh size of topography measurements was 10 cm and 1.6 cm in the streamwise and spanwise directions, respectively.

3.2. *Results of preliminary experiments*

For each experiment, suitable values of the governing parameters were chosen in order to produce values of β ranging from sub- to super-resonant conditions. Flow conditions are summarized in table 2, where D_m^* denotes the average water depth that was measured in the initial phase of the experiments, before the occurrence of bed deformation, and where the transport formula of Meyer-Peter and Müller, in the form given by Chien (1956) has been employed to compute resonant conditions. The values of the water (Q_l^*) and sediment (Q_s^*) discharges that fed the channel were calculated so as to achieve longitudinal equilibrium with the value of S that was imposed at the initial bed configuration. The procedure described in § 3.1 allowed us to ascertain the absence of any significant aggradation and/or degradation occurring along the

https://doi.org/10.1017/S0022112005003927 Published online by Cambridge University Press

flume. When the predicted value of the equilibrium slope did not correspond to the observations, the parameters were suitably adjusted and the experiment was repeated under equilibrium conditions.

Overdeepening was observed in all the runs, consistently with theoretical predictions: downstream overdeepening characterized bed topography in experiments 1 and 2 under sub-resonant conditions, whereas upstream overdeepening was observed in experiments 5, 6 and 7, characterized by super-resonant conditions. The analysis of the time-varying longitudinal bed profiles allowed us to filter out the effects of the migrating bars, coexisting with the steady topography in most experiments.

Proceeding from the straight to the curved reach, these bars invariably increased their migration speed, that was of the order of few $\mathrm{cm\,min^{-1}}$; moreover their wavelengths almost halved from 5–6 times the channel width in the upstream reach to 3–4 times in the bend.

In figure 4, two-dimensional pictures of the instantaneous bed topography measured by the laser scanning device at the end of run 5 and run 6 are reported. Upstream overdeepening is displayed by the significant deposit present at the inner bank and along the whole right-hand side of the straight reach in both runs 5 and 6. Such a configuration cannot be interpreted as a migrating bar since the average bed profiles analysis of figure 5 reveals the persistence of this transverse deformation in time. The wavelength of the latter can be estimated roughly around 10–12 times the flume width (note that the length of the upstream reach allowed us only to observe approximately half of the whole steady bar structure).

The wavelength characterizing such steady perturbation is then much longer than the typical wavelength of migrating bars forming under the conditions of the present experiments. Such steady bed deformation was completely absent in the upstream reach of the flume in experiments 1 and 2, carried out under sub-resonant conditions (figure 6). This was ascertained through visual observations of the bed profile on the sidewalls, which unfortunately have not been thoroughly documented in the sub-resonant runs. However, figure 6 provides some qualitative indication of the absence of upstream overdeepening in run 1 and in run 2. Finally, note that the average bed profiles of run 1 (figure 7) clearly indicate the presence of downstream overdeepening in the curved reach under sub-resonant conditions.

The above successful, yet qualitative, observations require some comments to point out further features of the phenomenon which complicate the overall picture.

(i) In the 270° flume, the end section did force a persistent local perturbation of bottom topography, as the bed was forced to keep flat in the transverse direction: this was a further mechanism which triggered the development of upstream overdeepening originating at the end section. This can be detected in figure 4. In other words, in the curved reach, steady bars are present under both sub- and super-resonant conditions: in the former case they originate at the junction of the straight and the curve and decay downstream; in the latter case they originate at the end section and decay upstream.

(ii) The straight reach upstream to the 270° bend was unfortunately not long enough to accommodate an entire bar wavelength, as clearly observed in figures 4 and 5. This prompted the need for repeating the experiment on a larger-scale facility. The U-shaped flume experiment described in § 4 fulfils the required conditions.

(iii) The theoretical prediction of the overdeepening phenomenon was obtained on the basis of a theory which ignored the possible coexistence of free migrating bars with the forced spatial bars induced by curvature. The present preliminary observations confirm the original suggestion of Kinoshita & Miwa (1974) according to which the

https://doi.org/10.1017/S0022112005003927 Published online by Cambridge University Press

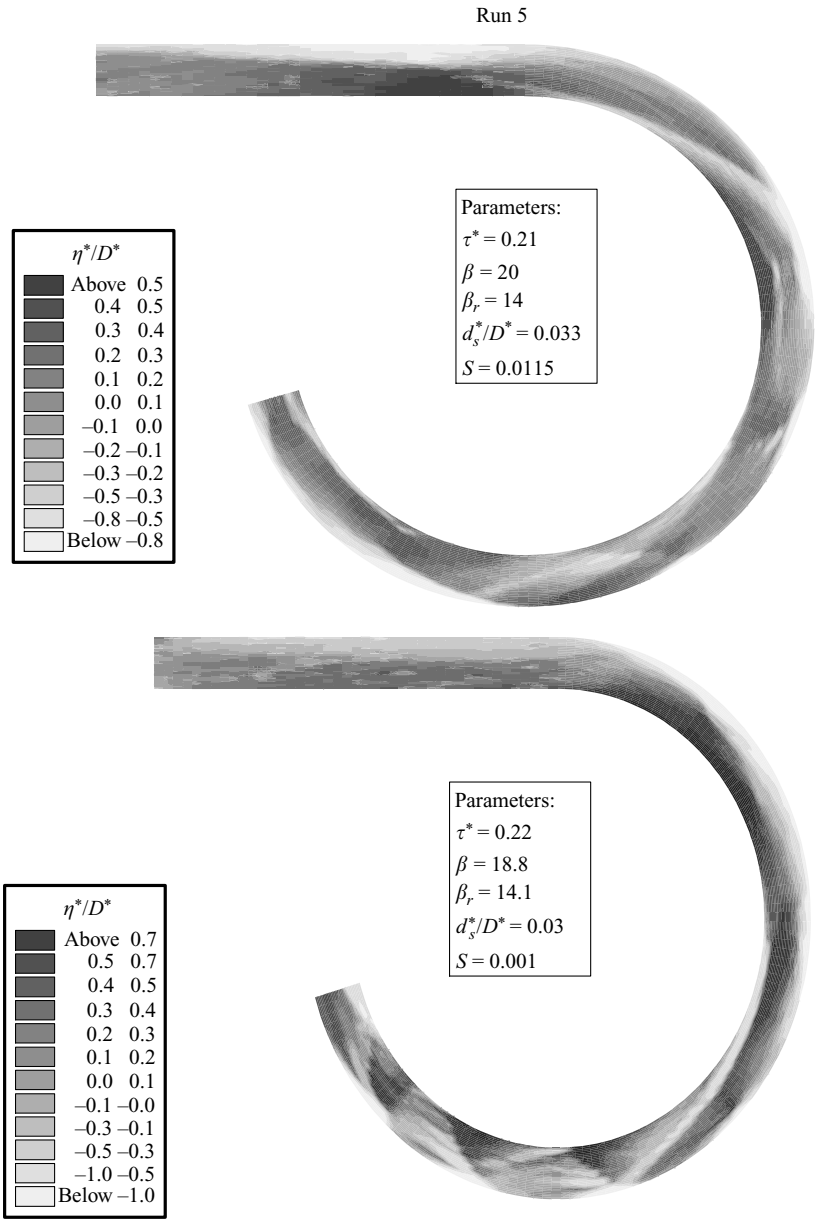


FIGURE 4. Bed topography measured at the end of runs 5 and 6 (super-resonant conditions).

presence of a single bend is unable to suppress the migration of free bars. Indeed, migrating alternate bars did coexist with forced bars in each run.

4. U-flume experiments

4.1. *U-shaped flume apparatus*

The second set of experiments was carried out in an indoor PVC U-shaped flume, 60 cm wide, consisting of two straight reaches connected by a 180° bend of constant

https://doi.org/10.1017/S0022112005003927 Published online by Cambridge University Press

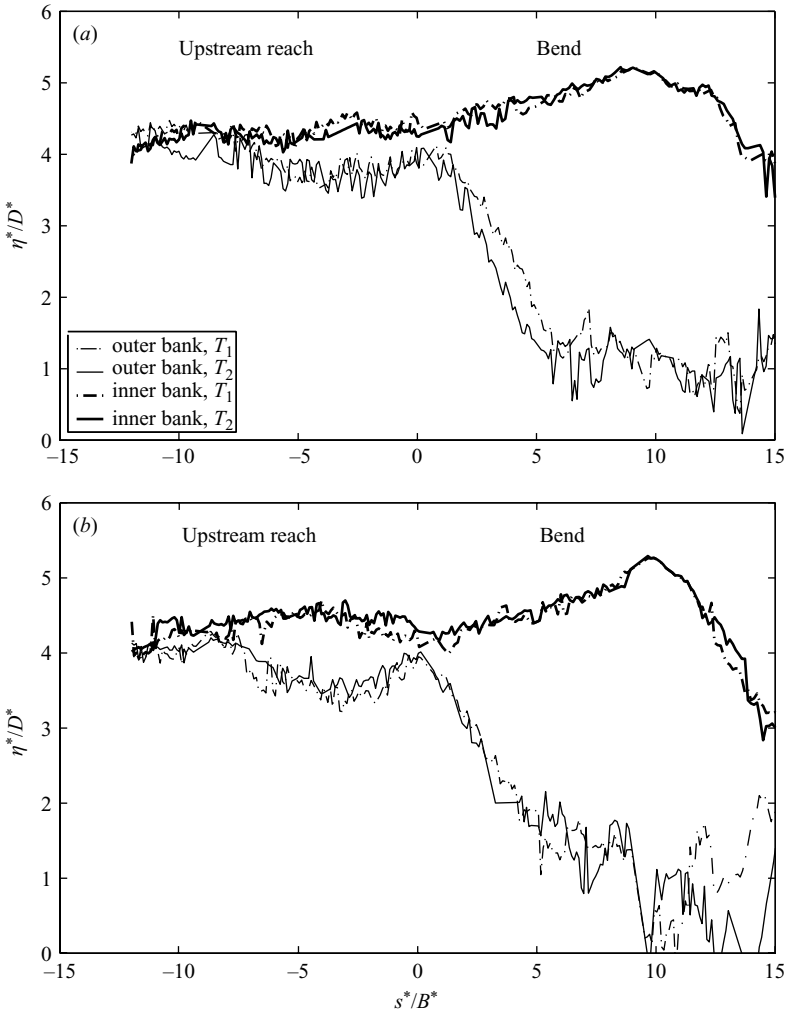


FIGURE 5. The inner and outer bank profiles computed averaging over two distinct bar periods in (*a*) run 5 and (*b*) run 6 (super-resonant conditions).

radius. The new flume was obtained by modifying the previous one; the upstream straight reach was lengthened by approximately 7 m and the bend was shortened by 90° to allow connection with the new downstream reach, 12 m long and parallel to the upstream one. The same inflow and outflow conditions, as in the previous set of experiments, were used. However, the downstream straight reach was now long enough to allow for the establishment of roughly uniform mean conditions such that the bed topography in the bend was essentially not affected by the end conditions. In this new set of experiments, both water and sediment (a coarser uniform sand with diameter $d_s^* = 1$ mm) were recirculated. At the downstream end of the flume, water and sand were first collected in a small settling tank, whose walls were impermeable to sediments, while water was discharged into a larger rectangular tank from which it was recirculated (figure 8*a*). From the smaller tank, sediments and some water were drained out by a cyclone pump (Struiksma 1985) and carried through a pipe to the flume inlet (figure 8*b*). Around 20–30 tetrapods, whose linear size was approximately

https://doi.org/10.1017/S0022112005003927 Published online by Cambridge University Press

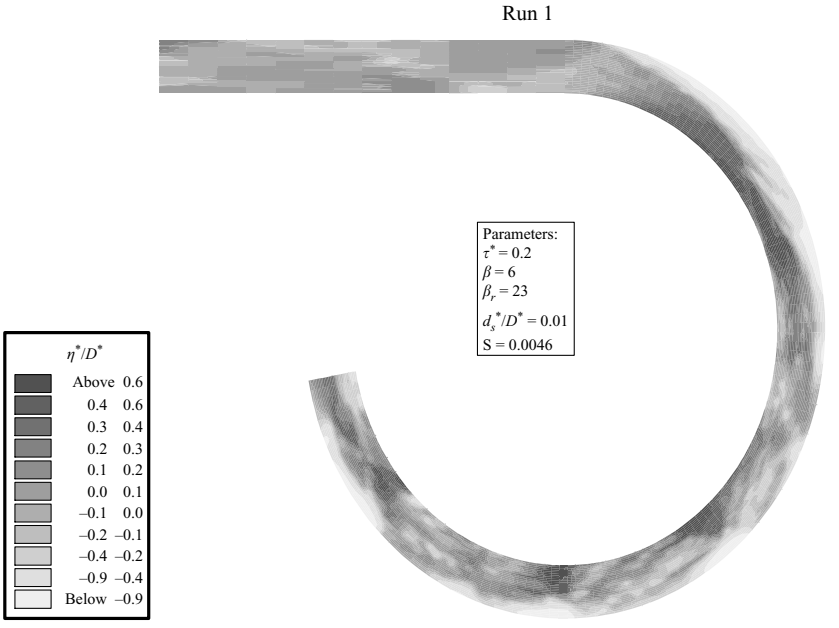


FIGURE 6. Bed topography measured at the end of run 1 (sub-resonant conditions).

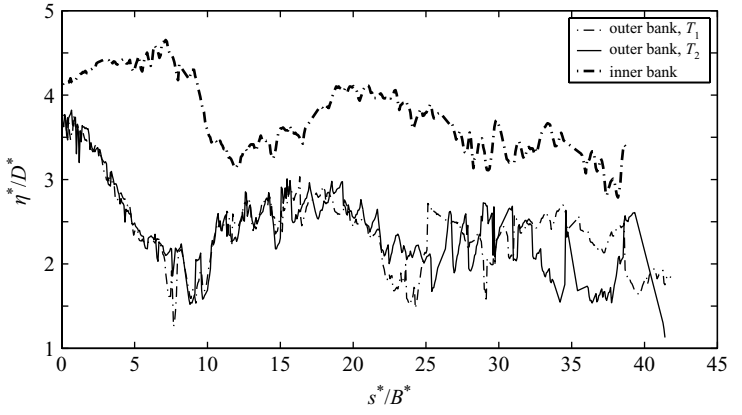


FIGURE 7. The inner and outer bank profiles computed averaging over two distinct bar periods in run 1 (sub-resonant conditions).

5 cm, were laid on the sand bed close to the flume inlet to avoid local erosion due to the falling jet of recirculated water–sediment mixture (figure 8*b*). A grid was also placed downstream in order to dissipate the local turbulence generated by the falling jet. The preparation and initial phase of the experiment, as well as the procedure whereby the bed slope was monitored and the bed topography was measured by the laser scanning device at the end of each run, were analogous to those employed in the previous set of experiments.

The measurement of the temporal development of bed topography throughout the channel was improved in the second set of experiments. In fact, in the previous

https://doi.org/10.1017/S0022112005003927 Published online by Cambridge University Press

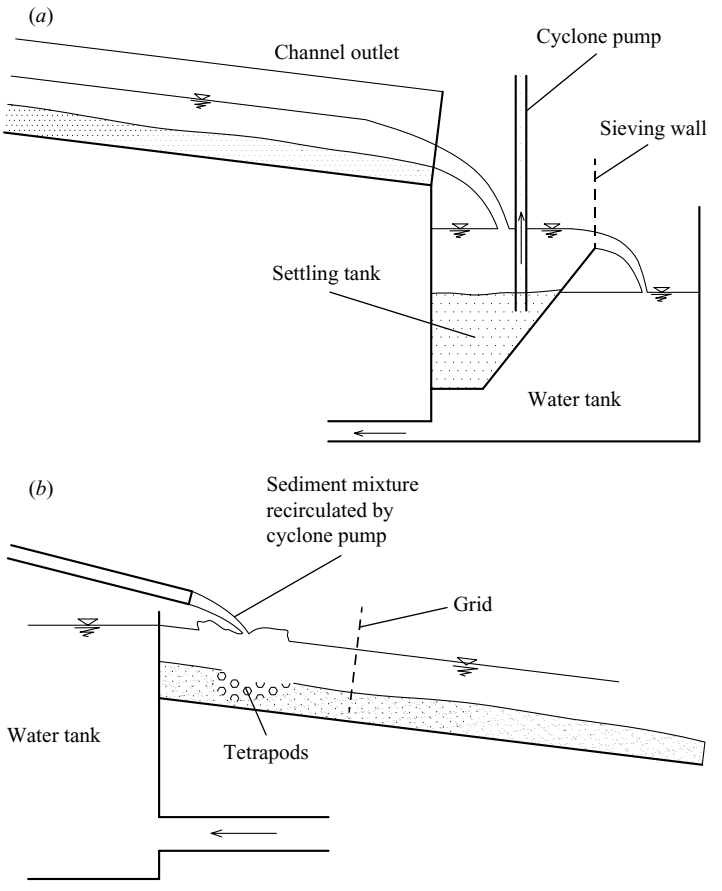


FIGURE 8. Sketch of (*a*) the outlet and (*b*) the inlet devices in the U-flume experiments.

set, only the steady component of the bed profile at the inner and outer banks had been sought. In the present set, the bed dynamics was monitored throughout the channel by means of a Profile indicator PV09 (Delft Hydraulics). This device has been designed so as to maintain a constant electric capacity (i.e. a constant vertical distance of roughly 1 mm) between the edge of the probe and the local bottom. Any local temporal variation of bed elevation was then registered by this instrument, with a rate of one measurement point per second. The time required to monitor bed topography in the straight reach was about 10 min, with measurements taken in cross-sections at a spacing of 1 m and including ten measurement points per cross-section.

Starting from the establishment of equilibrium conditions, experiments were carried on over a time interval larger than two periods of free bar migration. At the end of each experiment, the bed topography was measured by a laser scanning device mounted on the carriage: the tolerance of the scanner was 0.1 mm; the spatial mesh size of the topography measurement was 10 cm and 1.6 cm in the streamwise and spanwise directions, respectively.

4.2. *Data analysis*

The dimensionless parameters characterizing the U-flume experiments are reported in table 3. A few comments are in order. The values of β, d_s, F_o and τ_* are all based

https://doi.org/10.1017/S0022112005003927 Published online by Cambridge University Press

Run	U1	U2	U3	D1	D2
β	21.4	20.0	15.0	12.0	8.6
β_R	11.0	11.7	14.6	17.3	22.1
d_s	0.071	0.067	0.050	0.040	0.028
F_o	1.04	1.04	0.75	0.74	0.85
τ_*	0.093	0.1	0.133	0.167	0.233
D^* (cm)	1.4	1.5	2.0	2.5	3.5
Q_l^* l s^{-1}	3.25	3.6	4.0	5.5	10.5

TABLE 3. Relevant parameters of the U-flume experiments.

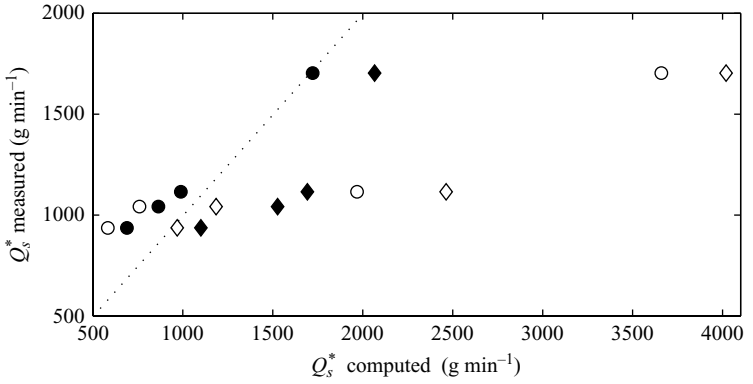


FIGURE 9. Comparison between the measured sediment rate and the computed values. ○, uniform, Parker predictor; ●, two-dimensional, Parker predictor; ◇, uniform, Meyer-Peter and Müller; ◆, two-dimensional, Meyer-Peter and Müller.

on the average uniform flow depth D^* measured in the straight reach in the initial phase of the experiments (when bars had not yet developed).

The calculation of the resonant value β_R depends on the choice of an appropriate transport law for sediments. We have then investigated which approach would fit the experimental values of the bedload discharge which was measured by a volumetric sampling technique. The comparison between the computed and the measured solid discharges has been carried out using two different procedures to calculate the sediment transport rate. On one hand, we have employed the values of τ_* for uniform flow in a rectangular cross-section reported in table 3 using Parker's (1990) predictor and the classical Meyer-Peter and Müller formula for the bedload transport rate. We have then tested a more accurate two-dimensional procedure accounting for the transverse and longitudinal variation of bed topography along the flume. Each cross-section along the flume was partitioned in narrow vertical strips employing the time-averaged bed topography. The bedload rate was then evaluated as the sum of the contributions associated with the local transport driven by the values of flow depth corresponding to locally uniform flow with the given water discharge. Figure 9 shows a comparison between the measured and the computed bedload rates employing both the former and the latter approach. It appears that calculation based on the uniform average flow in a rectangular cross-section provides a less satisfactory estimate of the bedload rate than the two-dimensional approach described above. Moreover Parker's

https://doi.org/10.1017/S0022112005003927 Published online by Cambridge University Press

predictor performs better than Meyer-Peter and Müller formula. Parker's predictor has then been chosen to calculate the resonant values of β_R reported in table 3.

In order to determine the steady component of the bed deformation to be compared with the theoretical results, the contribution of migrating bars to bed elevation was filtered out. In other words, the steady bed topography was obtained along the whole flume by time averaging the bed elevation at any location. As the time data set included more than one period of migrating bars, the averaging procedure was performed either over single or multiple periods, leading to almost identical results, thus confirming that the experiments had reached an average equilibrium configuration. The steady bed topography was finally analysed through a two-dimensional Fourier analysis performed separately for the straight and the curved reaches. This allowed us to calculate the wavelength and estimate all the harmonic contributions to the overdeepening oscillations.

The procedure consisted of two steps. First, the appropriate longitudinal size of the data set, corresponding to the wavelength of one steady bar unit, was chosen as the one which maximized the amplitude of the fundamental harmonic, associated with a two-dimensional alternate scour-deposition pattern that typically identifies the phenomenon under examination. Next, the two-dimensional power spectrum has been computed on the selected window. Note that the analysis was performed according to a classical procedure whereby the function $\eta(s, n)$ was extended symmetrically over one bank in the transverse direction, doubling the width of the channel such that it was possible to associate the alternate bar pattern with the first transverse mode. The same sequence was applied to the analysis of the bed topography measured at the end of each run through the laser scanning device, and allowed us to detect the wavelength of migrating bars.

4.3. *Description of the experiments*

The slope of the sand bed was fixed at 1.1 % and kept constant for each experiment. Hence, it was possible to move from sub- to super-resonant conditions by decreasing the water discharge and, consequently, the average flow depth D^*. Such a relatively high value of the bed slope was chosen in order to allow for sediment transport to occur even for low values of D^*, i.e. of the Shields stress τ_*. Five experiments were carried out under the conditions reported in table 3. Runs U1, U2 and U3 correspond to super-resonant conditions, while runs D1 and D2 correspond to sub-resonant conditions. The water depth was measured at the initial stage of each run before the bed was subject to deformation, associated with forced and migrating bars.

Experiments performed under super-resonant conditions were characterized by a similar bed dynamics, except for run U1 where transport was not observed in some regions of the upstream straight reach once the bed deformation was established: over bar tops the Shields stress periodically fell below the critical value for sediment transport, thus making the latter regions inactive. In the super-resonant runs bar migration took place along the whole flume, but diagonal fronts were not always clearly distinguishable as their amplitude was small with respect to steady deformations. This feature appears to be related to the nonlinear interaction between migrating bars and steady features associated with the overdeepening phenomenon. The period of bar migration was estimated by examining the time evolution of bed elevation close to the banks where the alternation of pools and riffles gave rise to oscillations of significant amplitude. Such a period of migration was of the order of 2 h in both runs U2 and U3 (figure 10*a*), where an alternate steady transverse deformation

https://doi.org/10.1017/S0022112005003927 Published online by Cambridge University Press

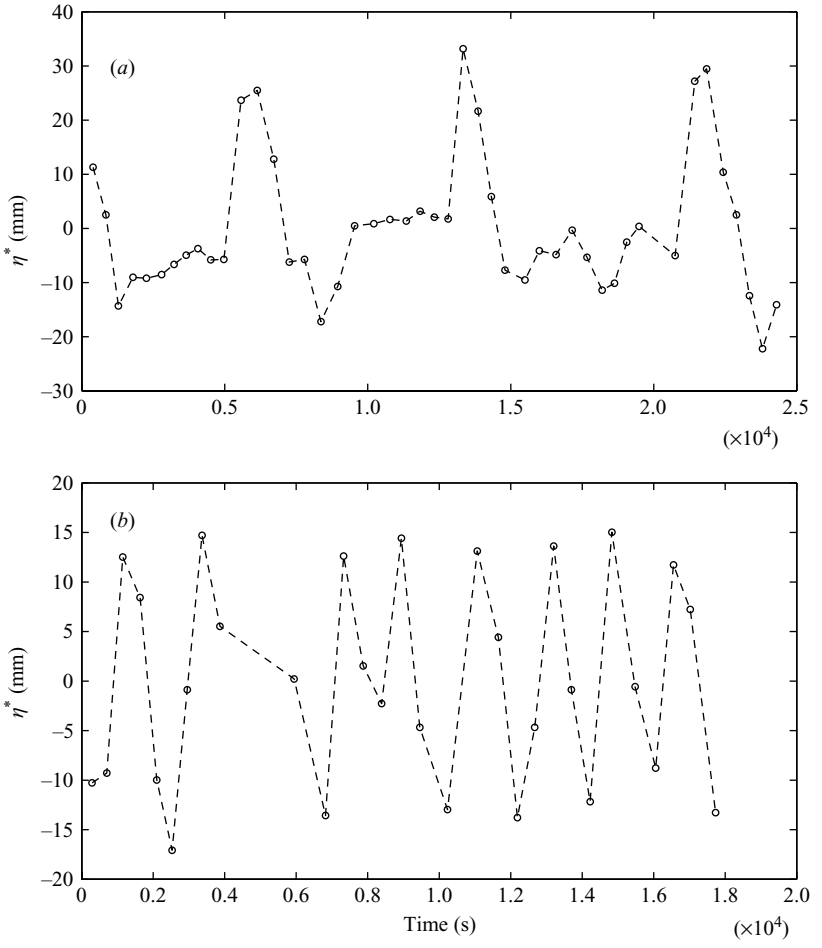


FIGURE 10. Time evolution of the bed topography close to the left bank in the upstream reach in (*a*) run U2 and (*b*) run D1.

of bed topography, with wavelength ranging about 8 m, was clearly detectable in the upstream reach. Figure 11, referring to the upstream reach, reveals the simultaneous presence of steady and migrating bars. Note the presence of persistent scour holes on the left bank at the beginning of the reach and on the opposite side, a few widths upstream of the bend entrance. The simultaneous migration of free bars is detected from the slower progressive shift of further scour holes in the planform sequence. On the contrary, no steady transverse perturbation of bed topography was observed in the upstream reach in the sub-resonant run D1 (figure 12), characterized by a faster bar migration with time periods of about 40 min (figure 10*b*), owing to a larger value of τ_*.

The presence of the bend connecting the two straight reaches strongly affected the behaviour of alternate bars, as it regularly reduced both wavelength and migration speed, their period keeping almost constant. The wavelength of migrating bars was approximately 6–7 times the flume width in the straight reaches under sub-resonant conditions, and the ratio reduced to 4–5 in the bend; in the super-resonant runs the above values increased by 10–20 % . Run D2 was characterized by the lowest

https://doi.org/10.1017/S0022112005003927 Published online by Cambridge University Press

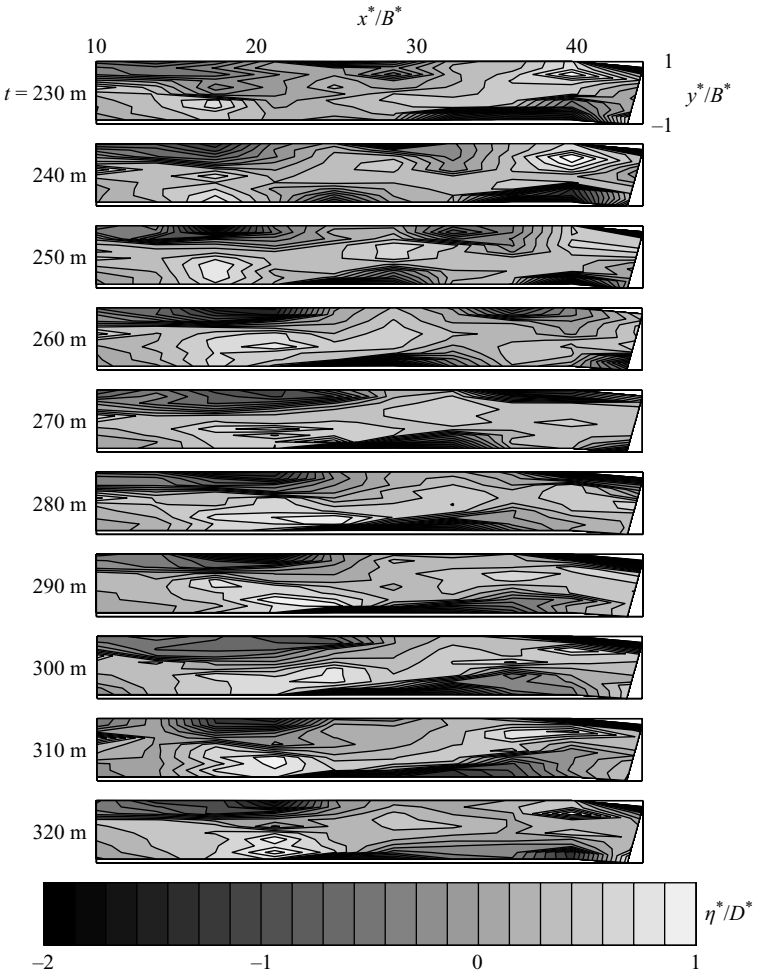


FIGURE 11. Time evolution of the bed topography in the upstream reach in run U2 (super-resonant conditions; flow from left to right).

value of β; bars did not form in the straight reaches, while antidunes were observed propagating downstream. Such bedforms were characterized by regular, nearly two-dimensional, bottom perturbations in phase with perturbations of the free surface (figure 13), wavelengths ranging about five mean flow depths and periods of about 20 s. Moreover, the particle Reynolds number based on friction velocity was about sixty, well within the range of the criterion for antidune formation predicted by Simons & Richardson (1961).

5. Theoretical interpretation of the U-flume experiments

The second series of experiments has allowed us to describe quantitatively the process of upstream overdeepening, whose existence had already been detected in the preliminary experiments carried out in the 270° flume. We now show that the theoretical work of ZS is able to correctly predict the conditions of occurrence, the pattern of bed deformation and the wavelength of upstream overdeepening observed

https://doi.org/10.1017/S0022112005003927 Published online by Cambridge University Press

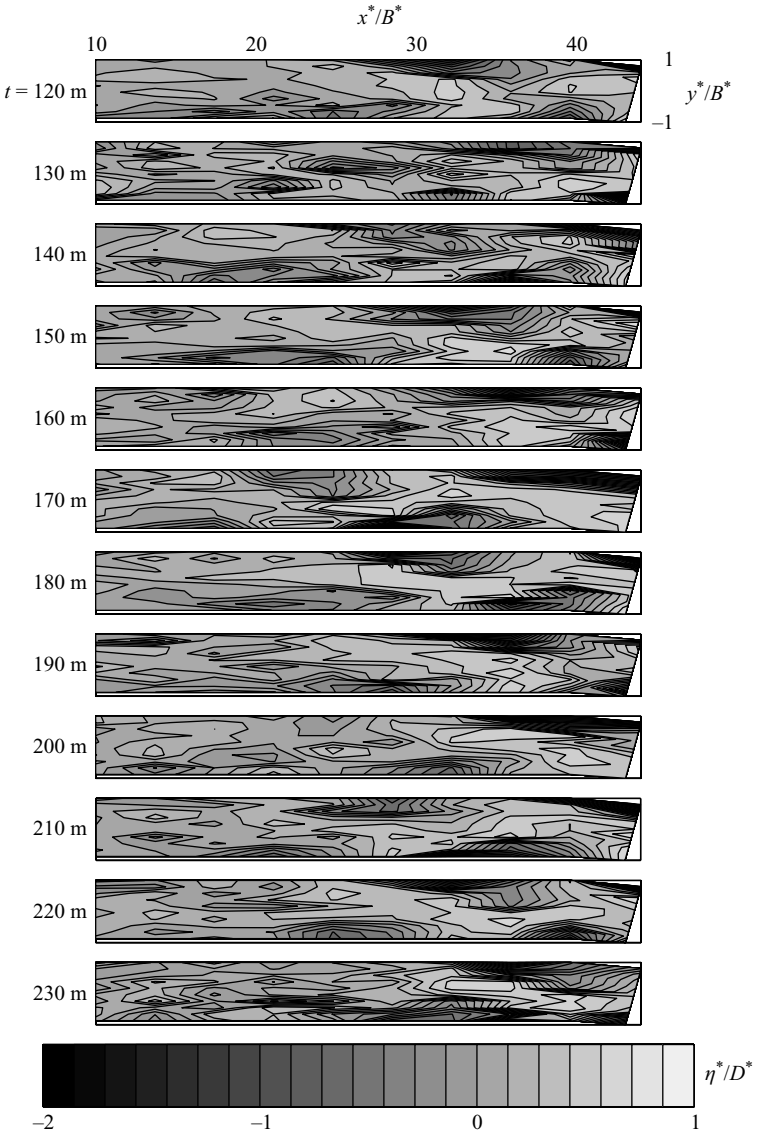


FIGURE 12. Time evolution of the bed topography in the upstream reach in run D1 (sub-resonant conditions; flow from left to right).

in the experiments. We will focus separately on the three channel reaches: upstream straight, curved and downstream straight.

The theory of ZS shows that upstream influence takes place only under super-resonant conditions: this has invariably been confirmed through observations in the upstream straight reach, where a steady bed deformation was detected only in runs U1, U2 and U3. On the contrary, in runs D1 and D2 no significant steady bed deformation was detected in the same reach. Examples of the steady patterns of bed topography are shown in figures 14 and 15 for runs U2, U3 and D1, D2 respectively, confirming that overdeepening is associated with an alternate bar configuration. This is consistent with the theory of ZS, which states that the expected bed deformation

https://doi.org/10.1017/S0022112005003927 Published online by Cambridge University Press

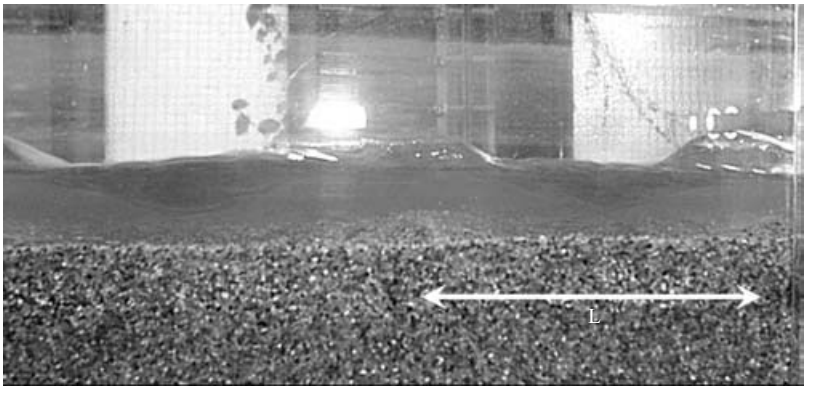


FIGURE 13. Lateral view of antidunes forming in the straight reach in run D2 (flow from left to right).

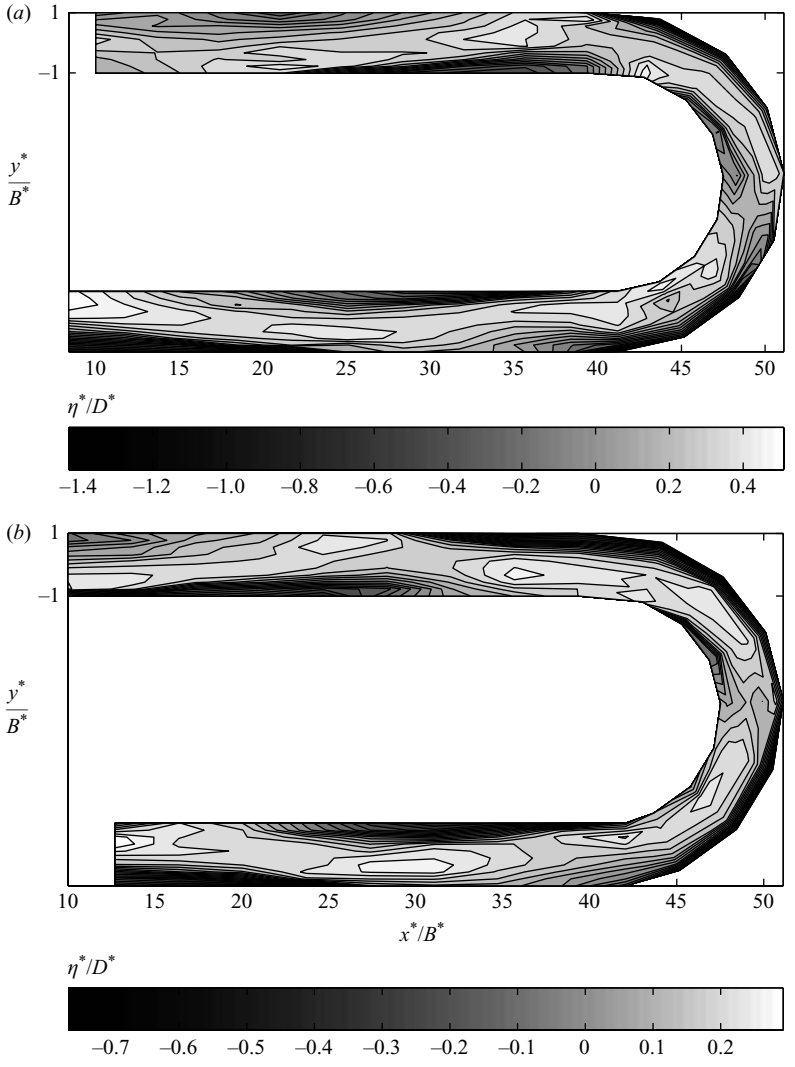


FIGURE 14. Steady bed topography under super-resonant conditions: (*a*) run U2 and (*b*) run U3. (Flow from top to bottom in these and in the following contour maps.)

https://doi.org/10.1017/S0022112005003927 Published online by Cambridge University Press

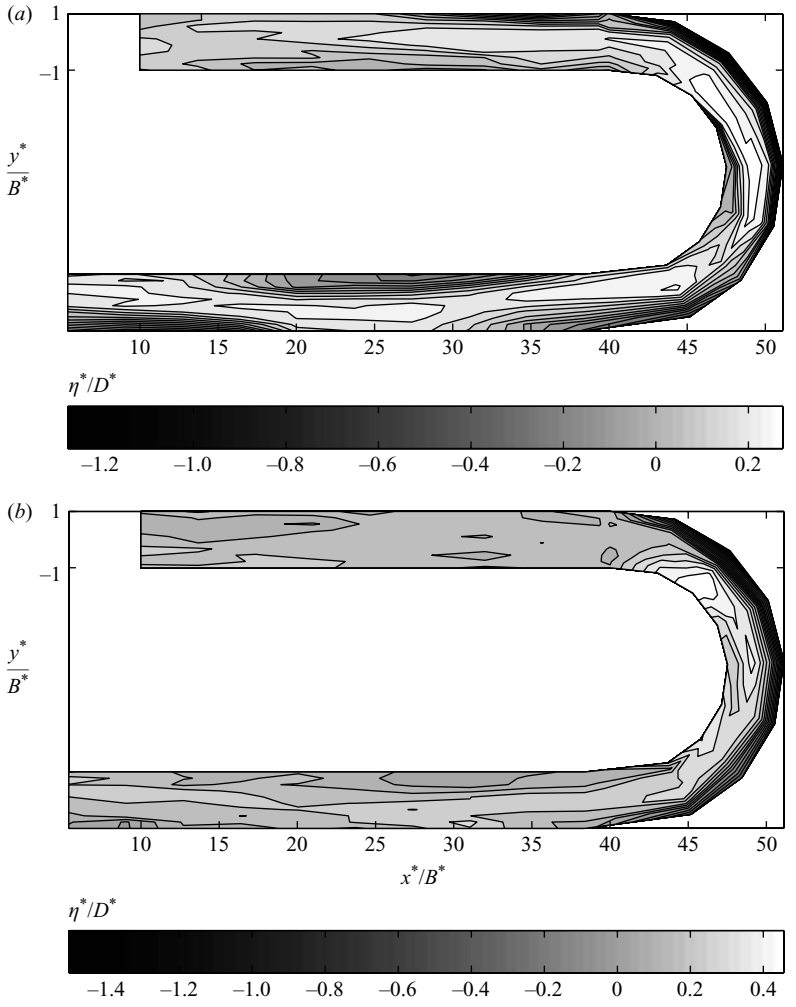


FIGURE 15. Steady bed topography under sub-resonant conditions: (*a*) run D1 and (*b*) run D2.

associated with upstream overdeepening consists of a classical alternate bar pattern, provided the width ratio of the channel is not so high that the second transverse mode (central bar) becomes super-resonant. The experimental conditions of runs U1, U2 and U3 are such that only for the first mode ($m = 1$) is β larger than β_R^m. These observations are confirmed by the two-dimensional Fourier analysis of the steady bed deformation. Figure 16 refers to the steady bed deformation that occurred in the upstream reach in run U2. Bed deformation is essentially due to the contribution of two largely dominant harmonics, the 1–1 and the 0–2. Note that the i–j harmonic indicates the Fourier component corresponding to the ith longitudinal mode and the jth transverse mode. Thus harmonic 1–1 corresponds to an alternate sequence of riffles and pools, while the 0–2 pattern is a longitudinally uniform central deposit (or scour). The latter is triggered by migrating alternate bars through nonlinear effects (e.g. Colombini *et al.* 1987). This further validates the theory of ZS, which predicts that upstream overdeepening in runs U2 and U3 is due only to an alternate bar

https://doi.org/10.1017/S0022112005003927 Published online by Cambridge University Press

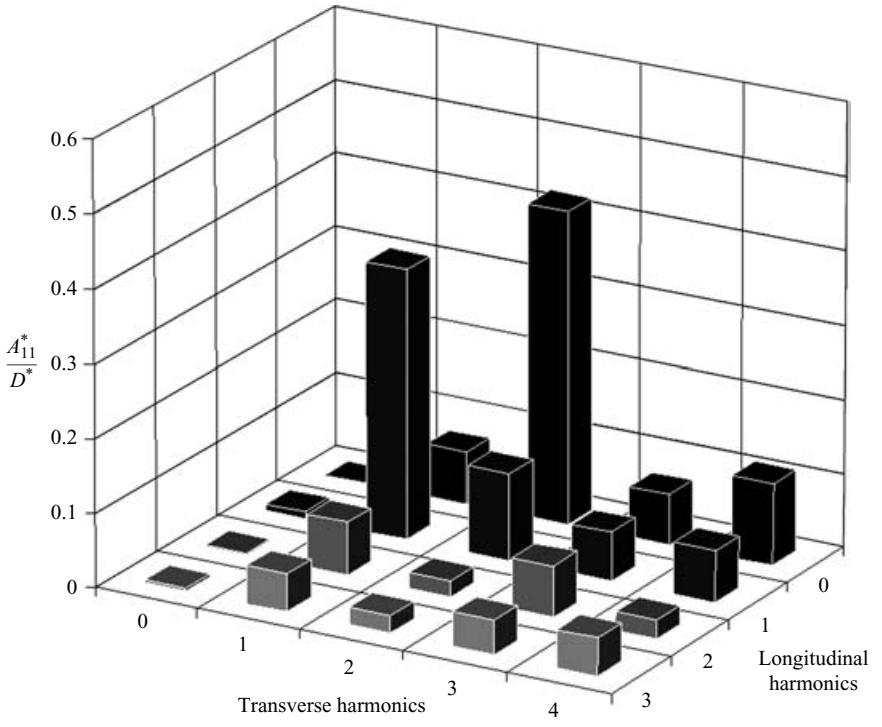


FIGURE 16. Two-dimensional Fourier spectrum of the dimensionless bed topography: upstream reach under super-resonant conditions (run U2).

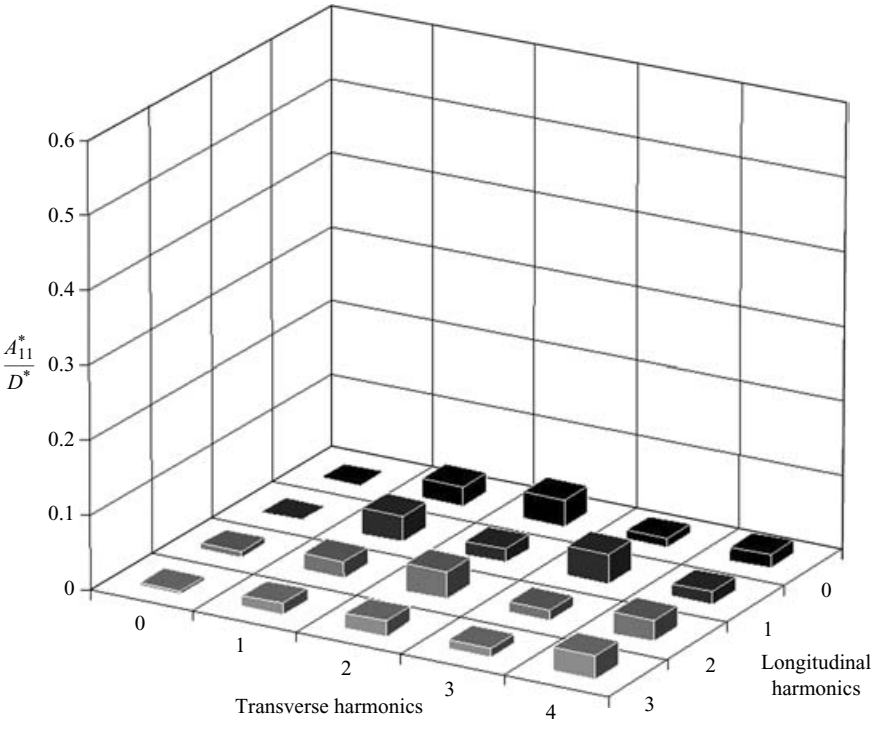


FIGURE 17. Two-dimensional Fourier spectrum of the dimensionless bed topography: upstream reach under sub-resonant conditions (run D2).

https://doi.org/10.1017/S0022112005003927 Published online by Cambridge University Press

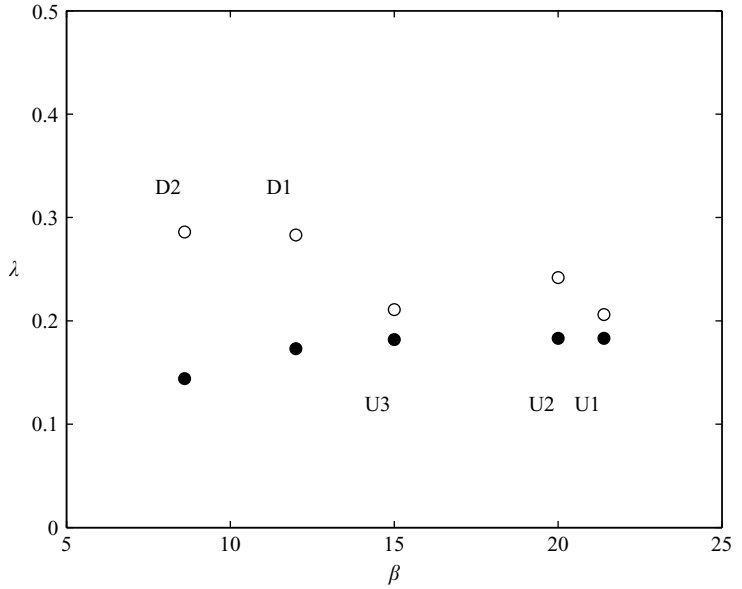


FIGURE 18. Comparison between the observed and predicted wavenumbers of overdeepening: ○, experiments; ●, theory.

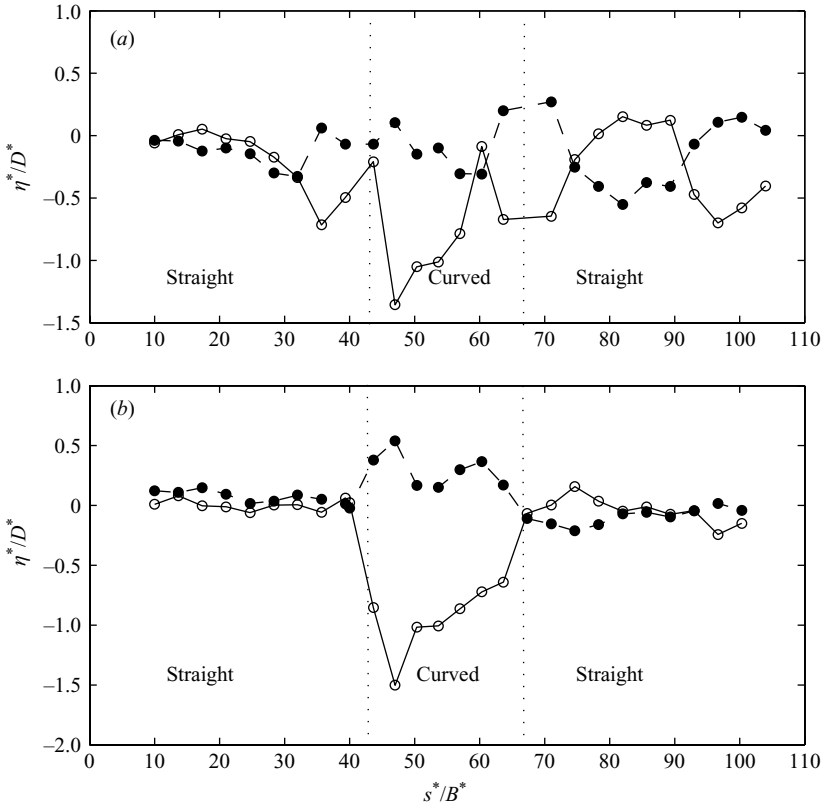


FIGURE 19. Steady bed profiles close to the ○, left and ●, right bank under sub-resonant conditions. (*a*) Run D1; (*b*) run D2.

https://doi.org/10.1017/S0022112005003927 Published online by Cambridge University Press

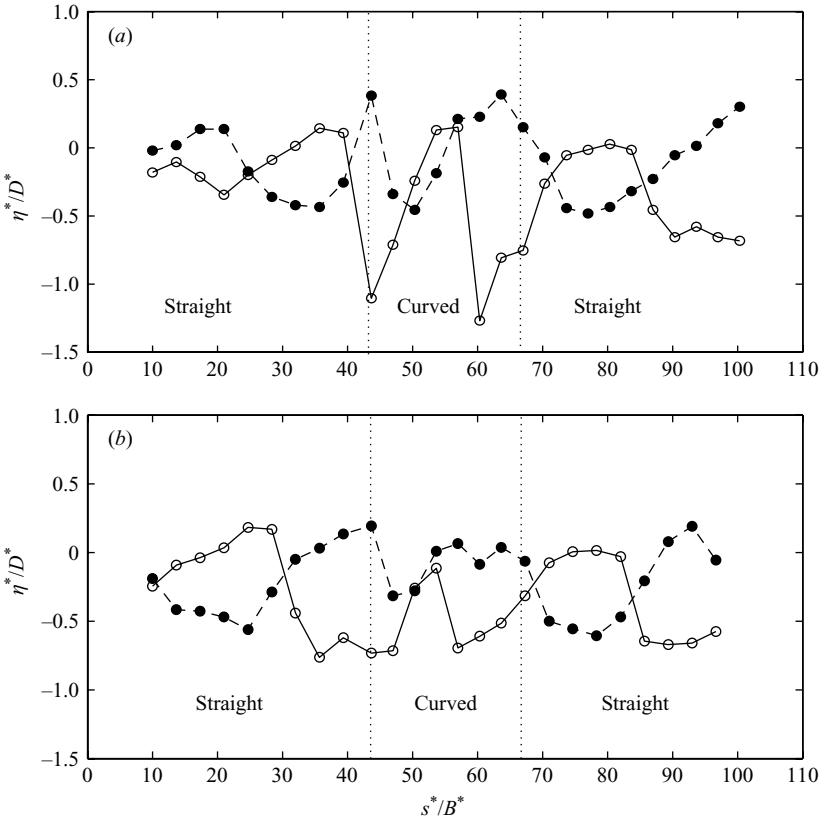


FIGURE 20. Steady bed profiles close to the ○, left and ●, right bank under super-resonant conditions. (*a*) Run U2; (*b*) run U3.

configuration. Moreover, the same Fourier analysis carried out in the same reach for the sub-resonant runs confirms the absence of significant steady bed deformation under sub-resonant conditions (figure 17).

Figure 18, shows a comparison between the values of the dimensionless wavenumber of overdeepening ($\lambda = 2\pi/(L^*/B^*)$) predicted by ZS and those calculated from the present experimental data. Such a calculation has been performed according to the procedure described at the end of § 4.2. The comparison in figure 18 concerns the wavenumbers of upstream overdeepening for runs U1, U2 and U3, whereas in the case of runs D1 and D2 it refers to downstream overdeepening. It appears that the predictions are satisfactory in the super-resonant case, whereas the wavelength ranged about 9 m (hence smaller than the length of the straight reach). Less satisfactory is the comparison for the sub-resonant case where theory predicts values of the wavelength which exceed the length of the downstream straight reach. Finite-length effects may then be the cause of such discrepancy.

The U-flume experiments allow us to further clarify the main differences of the channel bed dynamics under sub- and super-resonant conditions.

Overdeepening takes place in the downstream reach when $\beta < \beta_R$ (see figure 15 and the longitudinal bed profiles of figure 19): this is in agreement with the theory of ZS and with theoretical and experimental observations of Struiksma *et al.* (1985).

https://doi.org/10.1017/S0022112005003927 Published online by Cambridge University Press

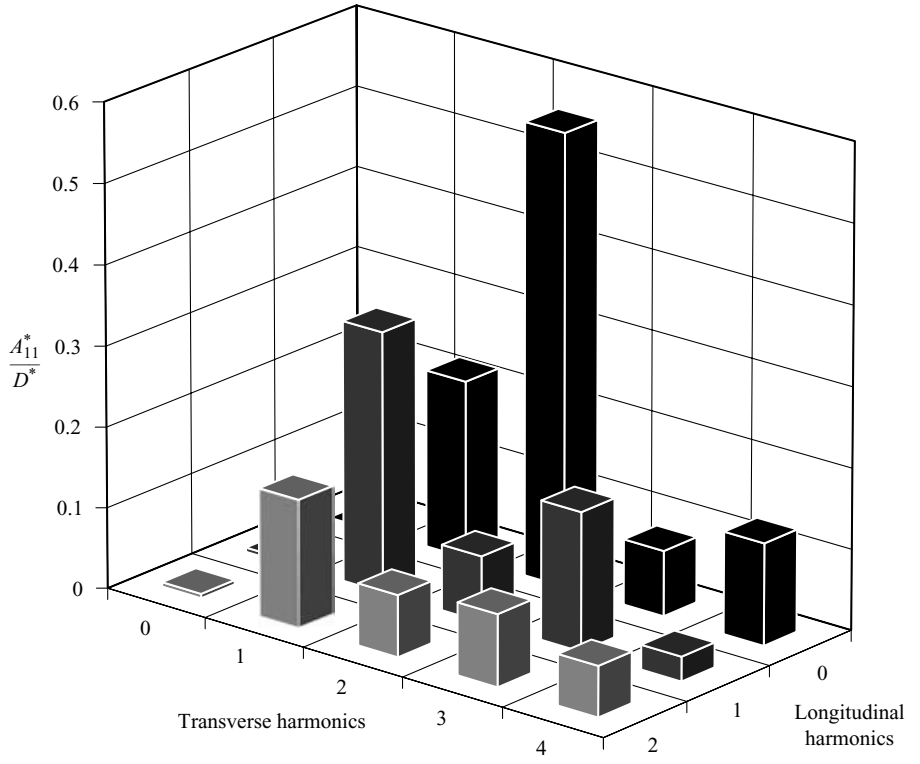


FIGURE 21. Two-dimensional Fourier spectrum of the dimensionless bed topography: downstream reach under super-resonant conditions (run U2).

A significant steady bottom deformation is detected in the same reach also under super-resonant conditions, as shown in the figures 14 and 20; the latter result is also in agreement with the theory of ZS. However, note that the latter predicts that downstream overdeepening under super-resonant conditions only leads to the presence of sub-resonant transverse modes, i.e. modes higher than the first, for the conditions of runs U1, U2 and U3. On the contrary, our observations show that the Fourier spectrum of the steady bed topography in the same reach (figure 21) contains also a significant contribution of the first mode whose amplitude is comparable with those associated with higher transverse modes. This feature cannot be predicted by the theory of ZS: indeed, in a linear context, the exponentially growing first mode cannot be included in the downstream reach as it does not keep bounded at infinity. However, the work of Seminara & Tubino (1992) has clarified that such modes evolve towards a finite amplitude if nonlinear effects are accounted for. A fully nonlinear numerical solution is then called for in order to provide a complete interpretation of the experimentally observed patterns.

A similar behaviour arises when examining the longitudinal bed profiles in the curved reach (figures 19 and 20). Bed overdeepening is triggered by curvature discontinuities occurring at the entrance and at the exit of the bend. When β is lower than β_R (figure 19) this is displayed by a deeper scour hole close to the outer bank located immediately downstream of the bend entrance and by a corresponding deposition close to the opposite bank: the above perturbation then decays longitudinally along

https://doi.org/10.1017/S0022112005003927 Published online by Cambridge University Press

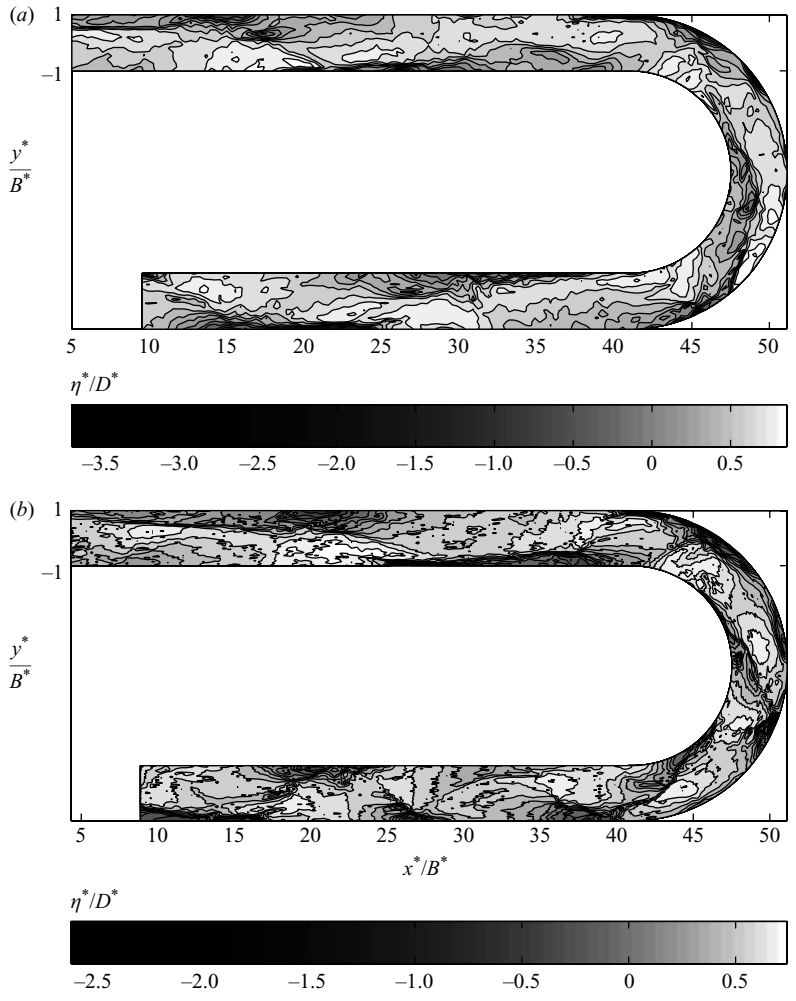


FIGURE 22. Instantaneous bed topography measured at the end of (*a*) run U1 and (*b*) run U2 by the laser scanning device.

the curved reach; this is reproduced by the classical two-dimensional models (e.g. Struiksma *et al.* 1985) and also by ZS. Under super-resonant conditions (figures 20), the scour regions are observed also immediately upstream of the bend exit, suggesting that the curved reach exhibits both upstream and downstream overdeepening triggered by the two curvature discontinuities.

The simultaneous presence of migrating and steady bars has also been monitored at the end of each experiment by the laser scanning device. The instantaneous bed topography corresponding to super-resonant conditions (runs U1 and U2) and to sub-resonant conditions (runs D1 and D2) is reported in figures 22 and 23, respectively. A spatial density high enough to estimate the contributions of both steady and migrating bars in a wavelength domain had to be employed. It is instructive to compare the instantaneous and the time-averaged bed topographies for the same experiments.

The bars appearing in the upstream reach of run D1 (figure 23) are not associated with overdeepening, as the corresponding average topography displayed in figure 15

https://doi.org/10.1017/S0022112005003927 Published online by Cambridge University Press

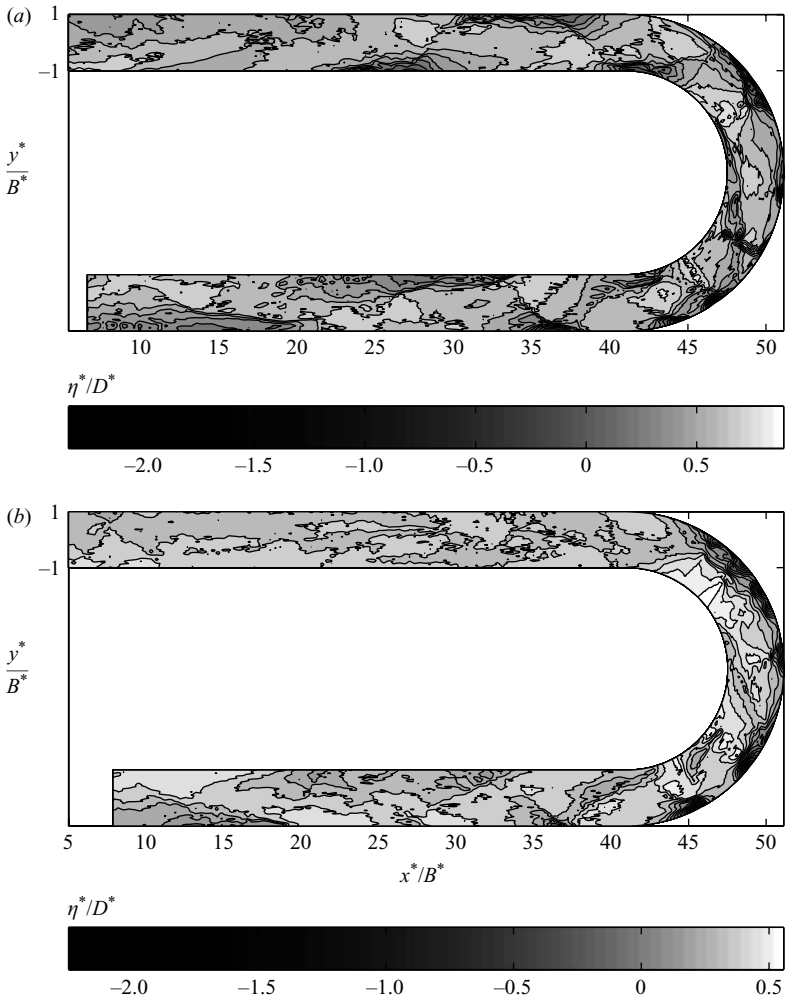


FIGURE 23. Instantaneous bed topography measured at the end of (*a*) run D1 and (*b*) run D2 by the laser scanning device.

reveals the absence of any steady perturbation with an alternate pattern. Moreover, the wavelength of these bars is much smaller than the typical length of overdeepening, as also confirmed by the Fourier analysis reported in figure 24 (solid curve). Figure 24 refers to the first step of the analysis described at the end of §4.2. It shows the dimensionless amplitude of the fundamental Fourier component (corresponding to an alternate bar pattern) as a function of the selected wavenumber in the upstream reach for different runs. The peak of these curves corresponds to the actual wavenumbers of the dominant alternate bar perturbation occurring in each experiment. The wavenumber of bars that appear in the upstream reach of run D1 (figure 23) corresponds to the typical value of free migrating bars (around 0.4), confirming the migrating nature of D1 bars. A similar comparison performed for run U2, again allows us to distinguish between the migrating and the steady contributions (see figures 22 and 14).

https://doi.org/10.1017/S0022112005003927 Published online by Cambridge University Press

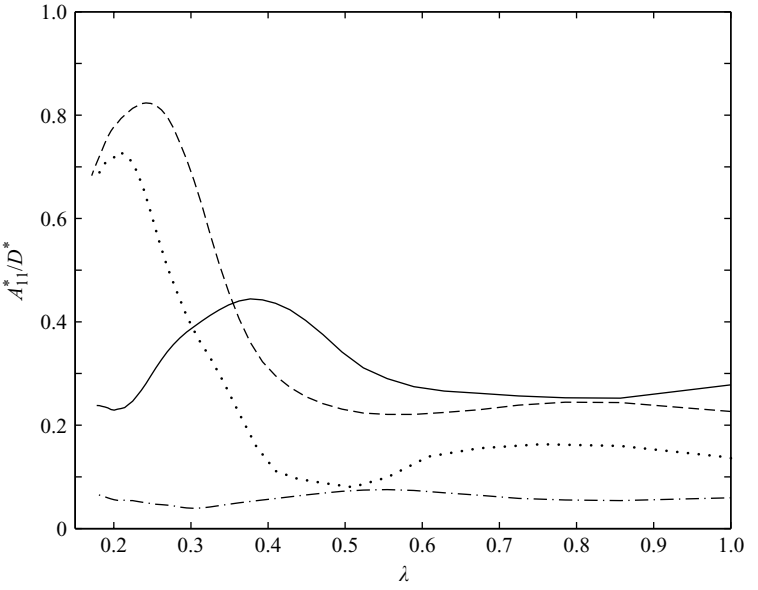


FIGURE 24. The amplitude of the fundamental harmonic under sub- and super-resonant conditions in the upstream straight reach is plotted for different runs versus the wavenumber of the chosen window. . . ., U1; - - -, U2; —, D1; -·-, D2.

6. Final remarks

The experimental observations discussed in this paper conclusively confirm the theoretical predictions of ZS, which suggested that the presence of geometrical discontinuities in meandering and straight rivers, in particular a discontinuity in channel curvature, is only felt downstream in sufficiently narrow channels ($\beta < \beta_R$) while it dominantly affects the upstream reach in wider channels ($\beta > \beta_R$). A second observation has confirmed a conclusion previously reached by Kinoshita & Miwa (1974): a single bend is unable to suppress the migration of free bars. In fact, in each run of the present series of experiments, free migrating alternate bars did coexist with the steady bars forced by curvature as well as with the steady spatially oscillating bars associated with downstream or upstream overdeepening. Distinguishing the steady component of the perturbation from migrating features has required the filtering procedures discussed in §§ 3.1 and 4.2.

Various practical and conceptual implications of the phenomenon of upstream overdeepening will have to be further explored in the future:

(i) When designing regulation works in wide channels, one should be aware that the upstream reach may be affected by the development of steady bottom perturbations, which might require the extension of bank protection upstream.

(ii) Upstream influence modifies the nature of the planimetric evolution of meandering rivers which may display downstream skewing and upstream migration of large-amplitude meanders, as discussed by Seminara *et al.* (2001).

(iii) The choice of boundary conditions for numerical models of river morphodynamics must account for the possible occurrence of the upstream overdeepening phenomenon, an issue that may be of particular relevance for braided rivers.

As mentioned in § 5, a complete understanding of the complex pattern observed in the present experiments will ultimately require the development a fully nonlinear

https://doi.org/10.1017/S0022112005003927 Published online by Cambridge University Press

(necessarily numerical) model, able to include the effect of bar perturbations, that grow exponentially in the linear regime covered by ZS, but develop a finite amplitude, i.e. a bounded response, in the weakly nonlinear regime investigated by Seminara & Tubino (1992). Such a model will also allow us to describe the nonlinear interactions between steady and migrating features obviously ignored in the linear model of ZS.

The experimental work has been initially jointly supported by the Italian Ministry for Scientific Research (MIUR) and by the University of Genova under the project 'Fluvial and coastal morphodynamics'. The work has been completed with the support of the RIMOF project and under the umbrella of the project 'Morfodinamica di reti fluviali – COFIN 2001' jointly supported by MIUR and various Italian universities, including Genova, Trento and Palermo. The contribution of G. Zolezzi to the preparation of the manuscript has been carried out also in the context of CUDAM – University of Trento.

REFERENCES

Biederharn, D. S., Raphelt, N. & Montague, C. 1983 Long term stability of the Oachita River. In *River Meandering: Proc. of the Conference Rivers'83* (ed. Charles M. Elliot). ASCE.

Blondeaux, P. & Seminara, G. 1985 A unified bar-bend theory of river meanders. *J. Fluid Mech.* **157**, 449–470.

Chien, N. 1956 The present status of research on sediment transport. *Trans. ASCE* **121**, 833–868.

Colombini, M., Seminara, G. & Tubino, M. 1987 Finite-amplitude alternate bars. *J. Fluid Mech.* **181**, 213–232.

De Vries, M. 1973 Riverbed variations. Aggradation and degradation. *International IAHR Seminar on the Hydraulics of Alluvial Streams*. New Delhi.

Engelund, F. & Hansen E. 1967 *A Monograph on Sediment Transport in Alluvial Streams*. Danish Technical Press, Copenhagen.

Gilvear, D., Winterbottom, S. & Sichingabula, H. 2000 Character of channel planform change and meander development: Luangwa River. *Earth Surface Proc. Landforms* **25**, 421–436.

Ikeda, S. 1989 Sediment transport and sorting at bends. In *River Meandering* (ed. S. Ikeda & G. Parker). Water Res. Monograph **12**, pp. 103–126. Am. Geophys. Union. Washington DC.

Ikeda, S., Parker, G. & Sawai, K. 1981 Bend theory of river meanders. Part 1. Linear development. *J. Fluid Mech.* **112**, 363–377.

Johannesson, J. & Parker, G. 1989 Linear theory of river meanders. In *River Meandering* (ed. S. Ikeda & G. Parker). Water Res. Monograph **12**, Am. Geophys. Union, pp. 181–214. Washington DC.

Kinoshita, R. & Miwa, H. 1974 River channel formation which prevents downstream translation of transverse bars. *Shinsabo* **94**, 12–17 (in Japanese).

Klaassen, G. 2002 Novel approaches in river engineering. *Invited lecture at the Riverflow2002 Conf. Louvain La Neuve, Belgium, September* 3–6, pp. 27–44.

Lanzoni, S. 2000*a* Experiments on bar formation in a straight flume. 1. Uniform sediment. *Water Resourses Res.* **36**, 3337–3349.

Lanzoni, S. 2000*b* Experiments on bar formation in a straight flume. 2. Graded sediment. *Water Resources Res.* **36**, 3351–3363.

MacDonald, T. E., Parker, G. & Leuthe, D. P. 1991 Inventory and analysis of stream meander problems in Minnesota. *Res. Rep.*, St Anthony Falls Hydraulic Laboratory, University of Minnesota.

Monsalve, G. C. & Silva, E. F. 1983 Characteristics of a natural meandering river in Colombia: Sinu River. In *River Meandering: Proc. of the Conf. Rivers'83* (ed. Charles M. Elliot). ASCE.

Parker, G. 1990 Surface-based bedload transport relation for gravel rivers *J. Hydraul. Res.* **20**, 417–436.

Schielen, R., Doelman, A. & de Swart, H. 1993 On the nonlinear dynamics of free bars in straight channels. *J. Fluid Mech.* **244**, 325–356.

https://doi.org/10.1017/S0022112005003927 Published online by Cambridge University Press

Seminara, G. & Tubino, M. 1992 Weakly nonlinear theory of regular meanders. *J. Fluid Mech.* **244**, 257–288.

Seminara, G., Zolezzi, G., Tubino, M. & Zardi, D. 2001 Downstream and upstream influence in river meandering. Part 2. Planimetric development. *J. Fluid Mech.* **438**, 213–230.

Simons, D. B. & Richardson, E. V. 1961 Forms and bed roughness in alluvial channels. *J. Hydraul. Engng ASCE* **87**, HY3.

Struiksma, N. 1985 The cyclone pump. *J. Hydraul. Res.* **23**, 165–167.

Struiksma, N., Olesen, K. W., Flokstra, C. & De Vriend, H. J. 1985 Bed deformation in curved alluvial channels. *J. Hydraul. Res.* **23**, 57–79.

Tubino, M. & Seminara, G. 1990 Free-forced interactions in developing meanders and suppression of free bars. *J. Fluid Mech.* **214**, 131–159.

Whiting, P. J. & Dietrich, W. E. 1993 Experimental studies of bed topography and flow patterns in large-amplitude meanders. 1. Observations. *Water Resources Res.* **29**, 3605–3622.

Zolezzi, G. & Seminara, G. 2001 Downstream and upstream influence in river meandering. Part 1. General theory and application to overdeepening. *J. Fluid Mech.* **438**, 183–211.

https://doi.org/10.1017/S0022112005003927 Published online by Cambridge University Press